Photon antibunching as a probe of trajectory information of individual neutral atoms traversing an optical cavity

Zhiming Wu,* Shuting Shen, Jiahua Li,† and Ying Wu‡
School of Physics, Huazhong University of Science and Technology, Wuhan 430074, People's Republic of China

(Received 11 August 2021; revised 1 October 2021; accepted 3 November 2021; published 17 November 2021)

We present an alternative route to track the motion of a single atom traversing a high-finesse optical cavity by means of the coherence statistics of photon antibunching. Here the single atom strongly couples to the high-order transverse Laguerre-Gaussian (LG) mode (e.g., LG_{01}) of optical cavity, instead of the high-order transverse Hermite-Gaussian (HG) mode, which is beneficial to the single-atom trajectory measurement utilizing such a photon antibunching effect. With this aim, we characterize the position-dependent quantum correlations of the transmitted light in such a cavity quantum electrodynamics (QED) system subject to various kinds of the LG modes, finding that the photon antibunching effect is closely related to the position of the atom in the transverse plane and therefore the degree of the antibunching carries the information about the position of the atom within the cavity. The numerical results of the second-order correlation function agree well with the analytical calculations. Thanks to the tilted transverse LG_{01} mode of the cavity, which is inclined to the vertical direction by an angle of $\sim 15^{\circ}$, the LG-mode cavity QED architecture helps us to eliminate the degenerate trajectory of the single atom falling through the cavity and to obtain a unique atomic trajectory. In a 10-μs-long time interval as an example, our in-depth analysis displays that the atomic position with the spatial resolution of ~ 4.0 μm in the vertical direction (axis x) can be achieved. The present study is useful for well understanding and researching both the robust generation of single-photon source and the precision measurement of single-atom trajectory.

DOI: 10.1103/PhysRevA.104.053710

I. INTRODUCTION

Manipulation and measurement of individual atoms are significant for investigating the atom-photon interaction [1,2], atom-photon entanglement [3–5], quantum computing [6,7], and single-photon source preparation [8,9], just to mention a few. The deterministic control and measurement of single atoms are also essential preconditions for quantum logic operations [10] and quantum-information processing [11]. Up to now, two main avenues to gain information from a single atom have been favored in most experiments: one is to detect directly the atomic fluorescence signal which corresponds to the characteristic steps of individual atoms entering and leaving the trap [12–14]; the other is to observe the changes of light transmission through the cavity mirrors with strong atom-photon coupling [15–18]. Direct detection of single atoms through the collection of resonance fluorescence requires high-quality optical devices [12–14] and also the scattering section of single atoms is rather small, which make it difficult to sense the atom individually in free space. Alternatively, in order to perform the single-atom detection, one can monitor the transmission of a resonant cavity probe laser after dropping atoms from a magneto-optical trap (MOT) formed over the gap between the cavity mirrors [15–17]. However, the experiments based on the changes in the cavity transmission require strong atom-cavity coupling [19]. Cavity quantum electrodynamics (QED) provides an ideal platform for near deterministic control of the atom-photon enhanced interaction on the single-photon and single-atom level [20–22].

In a cavity QED regime of strong coupling, both the atom and the cavity have a damping rate smaller than the characteristic coupling coefficient of the combined atom-cavity system. In this scenario, even if only one photon or one atom enters into or escapes from the cavity mode, the state of the whole atom-cavity system can be completely modified [23,24]. In recent years, there has been considerable progress in integrating laser-cooled and trapped atoms with optical cavity QED systems in the strong-coupling regime [25–28]. The experiments performed with the laser-cooled atoms have demonstrated that individual atoms with a time resolution of a few microseconds can be observed [15,29,30], which is hard to imagine even for the most sensitive optical microscope. Beyond the realization of trapping, the high signal-to-noise ratio for continuous, real-time position measurement is itself one of the most significant characteristics of these strongly coupled cavity QED systems [31,32]. Such real-time detection capability enables the strongly coupled cavity QED systems to detect the position information of single atoms (see [33–35], and references therein).

We note that the forementioned works [33–35] about the single-atom detection focus mainly on the variations of the classical regimes in the transmission and reflection of the output field instead of quantum noises. However, the measurement of the single transit of the atom is relatively vulnerable to quantum noise in the experiment [33]. As shown in Ref. [33],

*zhiming@hust.edu.cn
†Corresponding author: huajia_li@126.com
‡yingwu2@126.com

utilizing photon antibunching can improve the signal-to-noise ratio of the transit signals, yet whether the coherence statistics of photon antibunching can reveal the information about the motion of a single atom in a given system remains mostly unexplored. Recently, great progress has been made in cavity QED consisting of an optical microcavity strongly coupled to a single atom, which can yield large optical nonlinearity even at the single-photon level [36–38] and induce an anharmonic Jaynes-Cummings (JC) ladder (i.e., the splitting between the dressed state energy levels is not constant) [39–42]. Correspondingly, this gives rise to a strong quantum correlation phenomenon, i.e., the so-called photon antibunching effect [43,44]. The photon antibunching effect with the strongly coupled interaction between the single atom and the cavity mode can produce a single-photon source [45–47], which plays an important role in quantum optics and quantum information technologies [48–51]. The coherent interaction of the atom and the cavity can significantly influence the coherent statistical properties of the output field in a high-finesse optical cavity. This influence is particularly large if the condition of strong coupling between the atom and the cavity is fulfilled. In this case, the coherence statistics of photon antibunching is a highly sensitive probe for the presence of an atom, so that efficient observation of a single moving atom becomes practical.

On the other hand, it is well known that the transverse amplitude distribution of the cavity modes is usually described by the Hermite-Gaussian (HG_{mn}) modes associated with TEM_{mnq} modes or the Laguerre-Gaussian (LG_{pl}) modes associated with TEM_{plq} modes (q is a constant, and $\{m, n\}$ and $\{p, l\}$ represent the orders of the HG and LG modes, respectively) [52,53]. The HG and LG modes are completely orthogonal solutions of Helmholtz equations in the Cartesian and cylindrical coordinates, which possess a rectangular matrix of intensity minima and maxima or a pattern of circular rings in the transverse plane [53]. However, for most of these experiments mentioned above, the atom is coupled to the HG modes. It is worth emphasizing that the coupling coefficient of the interaction between the cavity mode and the atom decreases with the increase of the order of the HG modes, which significantly reduces the contrast of the transit signals and degrades the detection of the atomic motion trajectory [33,35]. Applying the LG modes can help to improve these problems; especially in recent years, the LG modes can be used to track the motion of a single atom [54] and also find its significance in MOT [55]. On the one hand, since the field distribution of the LG modes is circular rings, when the atomic motion trajectory is near the circular edge, the small offset of the atomic position can cause a significant change of the coherence statistics of photon antibunching, which helps us to determine the atomic trajectory effectively. What is more, unlike the HG modes [33,35], the increase of the radial order p of the LG modes has little impact on the coupling coefficient between the cavity and the atom, which is beneficial to the mode selection of the LG modes and the maintenance of strong antibunching, and thus which can keep high contrast of the transit signals.

Inspired by this exciting development, here we put forward an alternative route to obtain two-dimensional (2D) position information of a single atom traversing the high-finesse optical cavity and utilizing the coherence statistics of photon antibunching in the LG-mode cavity QED system. Physically, the measurement scheme of the atomic trajectory information is based on the fact that the position of the atom within the cavity can lead to a significant influence on the coherence statistics of photon antibunching in the output field when a weak continuous-wave light is applied to coherently drive the LG cavity mode. That is to say, the value of the photon antibunching carries the information about the position of the atom. More specifically, by means of the two approaches [(i) the master equation approach and (ii) the Schrödinger equation approach], we present the detailed analytical and numerical results of the second-order intensity correlation function $g^{(2)}$, where the analytical results are in excellent agreement with the numerical simulations. With these methods at hand, using experimentally realistic parameters, we explore the position-dependent characteristics of antibunched photons from the three different LG modes in the cavity QED system, involving the LG_{00}, LG_{01}, and LG_{02} modes. In the atomic trajectory measurement scheme, we select the tilted LG_{01} mode to eliminate the degenerate trajectory of the single atom falling through the cavity and further obtain a unique atomic trajectory. By properly varying both the orders p and l of the LG modes in the coupled atom-cavity system, it is shown that strong antibunching in the LG modes can be well maintained, which is very favorable for the single-atom trajectory measurement. Based on the rotating frame coordinate transformation and the unique characteristics of this coupled system, the coherence statistics of photon antibunching can be used to characterize the trajectory of atom effectively. In a 10-μs-long time interval as an example, our in-depth analysis displays that an atomic position with the spatial resolution of $\sim$4.0 μm in the vertical direction (axis x) can be achieved with the experimentally achievable parameters. We also briefly discuss the feasibility of realizing this scheme experimentally in the LG-mode cavity QED device. Finally, we expect that our proposal may serve as a stepping stone to future theoretical and experimental investigations on the efficient generation of single-photon source and the precision measurement of single-atom trajectory.

The subsequent sections are organized as follows. In Sec. II, we describe the physical system of interest, pictorially represented in Fig. 1, and present the system Hamiltonian, where our physical model is taken into account under realistic experimental conditions in order to illustrate the effect of atomic motion on the photon antibunching. In Sec. III, we describe the physical quantities of our interest, namely, the second-order correlation function. Typically we yield insights into the numerical solution of the second-order correlation function via the master equation approach (Sec. III A) and the analytical solution via the Schrödinger equation approach (Sec. III B). In Sec. IV, we demonstrate the experimental feasibility of our proposed scheme and the choice of typical system parameters. All parameters discussed here are readily achievable experimentally. In Sec. V, we compare the analytical solution with the numerical solution and further analyze in detail the attainable results related to the position-dependent photon antibunching. Also, the effective

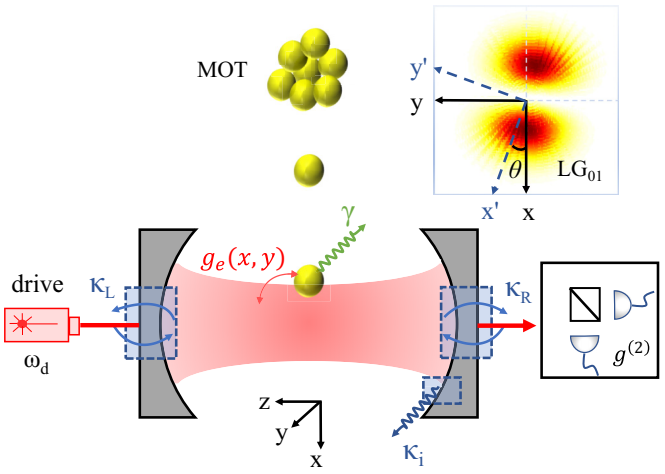

FIG. 1. Schematics of the LG-mode cavity QED system under study for probing the atomic trajectory information. The small golden filled circles represent the atoms (not to scale). The atoms fall down freely from MOT and a small fraction of these fall one by one through the mode of a high-finesse optical cavity. The cavity mode is a cylindrically symmetric LG_{01} mode in the transverse (x, y) plane and has a standing-wave structure in the axial (z) direction. The top-right inset denotes a tilted LG_{01} mode of the cavity from the front view (viewing along axial direction), where a rotating frame coordinate transformation is introduced. The cavity is coherently driven by an external laser field with the strength η and the central frequency ω_d via the left-hand mirror. The output field through the right-hand cavity mirror can be probed by measuring the normalized second-order intensity correlation function $g^{(2)}$. Here κ_L and κ_R are the damping rate of the left- and right-hand cavity mirrors, and κ_i is the inner cavity damping rate. The cavity is chosen to be symmetric, i.e., $\kappa_L = \kappa_R$. The total cavity damping rate is given by the sum $\kappa = \kappa_L + \kappa_R + \kappa_i$. Again $\kappa \gg \kappa_i$ holds, so κ_i can be ignored and we set $\kappa_i = 0$ in the following discussion without loss of generality. The effective coupling coefficient $g_e(x, y)$ is larger than cavity damping rate κ and atom damping rate γ, thus the interaction between the atom and the cavity mode can reach the strong-coupling regime. Other symbols are defined in the main text.

measurement of the atomic trajectory based on the photon antibunching is discussed in Sec. VI. Finally, the paper is summarized in Sec. VII.

II. PHYSICAL SYSTEM AND THEORETICAL FRAMEWORK

As depicted schematically in Fig. 1, we consider the LG-mode cavity QED system based on the JC-type model [56–58], consisting of an optical Fabry-Pérot cavity [19,59] and a single two-level atom (denoted by a ground state $|g\rangle$ and an excited state $|e\rangle$). The atoms can be collected in a MOT [60,61] directly above the center of the cavity, then fall freely under gravity and can be transversely placed in the center plane of a single higher-order transverse LG mode (such as LG_{01} mode; see inset of Fig. 1) with the resonance frequency ω_c.

At the position $(\vec{r}, z)$ along the cavity axis z, the electric field operator is proportional to $\hat{a}\cos(kz)f(\vec{r})\vec{\varepsilon}_x$ [62], where $\hat{a}$ is the annihilation operator of the cavity mode, $k = \omega_c/c$ (c is the speed of light), $f(\vec{r})$ is the transverse LG spatial mode profile, and $\vec{\varepsilon}_x$ denotes linear polarization in the x direction. Due to the existence of the radiation-pressure force exerted on the atom, the motion of the atom along the cavity axis z has an influence on the spectrum of quantum correlation $g^{(2)}$. However, considering that the cavity mode center is far away from the MOT in real experiments [15,34,35], the velocity of the atom in the cavity mode in the horizontal axial direction (axis z) is very small compared with that in the vertical direction (axis x), and the motion along the cavity axis z, which is likely pushed by the radiation-pressure force owing to an external weak laser field with frequency ω_d, is small [34,63]. In the present scheme, we consider the weak driving (weak excitation) case, where the intracavity field intensity is significantly small. Again, the radiation pressure force due to the cavity field is approximately proportional to the intracavity field intensity under this weak driving condition [64]. We thus can ignore the z-axis effect [i.e., $z \approx 0$ and $\cos(kz) \approx 1$; the atom passes through the antinode in a very narrow range in the axial direction and the radiation-pressure force exerted on the atom can be reasonably ignored] and assume that the atomic trajectory in the cavity mode is a vertical straight line. Also, the velocity of the atom entering and leaving the cavity mode under gravity changes little due to the fact that the distance between the MOT and the cavity mode is much larger than the size of the cavity mode, so the motion of the atom in the cavity mode can be assumed as uniform motion. If there is no trap in the cavity mode and the appropriate distance between the MOT and the cavity mode is selected, the single atom falling freely from the MOT into the cavity mode can be assumed as uniform motion and the atomic trajectory can be assumed as a vertical straight line, which is physically appropriate [34]. Finally through the right-hand cavity mirror we can probe the statistical characteristics of the output field by measuring the normalized second-order intensity correlation function $g^{(2)}$, and further determine the 2D position information of the atom.

To be specific, for a two-level atom coupled to a Fabry-Pérot cavity mode as shown in Fig. 1, the total Hamiltonian $\hat{\mathcal{H}}_{\rm tot}$ of the LG-mode cavity QED system within the electric-dipole and rotating-wave approximations reads (assuming $\hbar = 1$ here and hereafter)

$$\hat{\mathcal{H}}_{\rm tot} = \omega_c\hat{a}^\dagger\hat{a} + \omega_a\hat{\sigma}^\dagger\hat{\sigma} + g_e(x,y)(\hat{a}^\dagger\hat{\sigma} + \hat{a}\hat{\sigma}^\dagger) + \eta(e^{-i\omega_d t}\hat{a}^\dagger + e^{i\omega_d t}\hat{a}), \quad (1)$$

where $\hat{a}^\dagger$ and $\hat{a}$ are the creation and annihilation operators for photons inside the cavity obeying the bosonic commutation relations $[\hat{a}, \hat{a}^\dagger] = 1$, $[\hat{a}^\dagger, \hat{a}^\dagger] = 0$, and $[\hat{a}, \hat{a}] = 0$. $\hat{\sigma}^\dagger = |e\rangle\langle g|$ and $\hat{\sigma} = |g\rangle\langle e|$ are the Pauli raising and lowering flip operators of the two-level atom, satisfying the fermionic anticommutation relations $\{\hat{\sigma}^\dagger, \hat{\sigma}\} = 1$; $|e\rangle$ and $|g\rangle$ are the excited state and ground state of the two-level atom, respectively. The zero-point energy is set to the ground state $|g\rangle$. Ignoring the zero-point energy for the free cavity-field Hamiltonian is permitted because it only gives a relative shift and does not affect the system dynamics. ω_c is the resonance frequency of the cavity mode and ω_a is the transition frequency of the two-level atom. Lastly, ω_d and η are the central frequency and the strength of the external driving laser to motivate the cavity mode $\hat{a}$, respectively. The strength of the external driving

laser is given by $\eta = \sqrt{P_d \kappa_L/(\hbar\omega_d)}$, with P_d the pump power [65,66] and κ_L the cavity damping rate through the left-hand cavity mirror. The effective coupling coefficient $g_e(x, y)$ for the Fabry-Pérot cavity supporting the standing-wave mode with the LG transverse profile is determined by the actual position of the atom in the cavity mode:

$$g_e(x, y) = g_0 LG_{p,l}(r, \phi)/LG_{0,0}(0, 0). \tag{2}$$

Here, the maximum coupling strength g_0 between the cavity and the atom is proportional to $\sqrt{\omega_c/(2\hbar\varepsilon_0 V)}\vec{\varepsilon}_x \cdot \vec{\mu}_{eg}$, with ε_0 being the permittivity of vacuum, V the mode volume of the cavity, and $\vec{\mu}_{eg}$ the electric-dipole moment of the corresponding transition, respectively. Owing to the high speed of the atom itself and the fact that the absorption and emission of photons have little influence on their own speed, it can be considered that the driving laser has no influence on the motion of the atom, that is, the motion of the atom in the z direction is not taken into account. For convenience, we set the origin of coordinates at the center of the Fabry-Pérot cavity. In this circumstance, the antinode of the cavity mode is located at $z \approx 0$. We also set the electric-dipole moment $\vec{\mu}_{eg}$ to be parallel to the linear polarized direction $\vec{\varepsilon}_x$ of the electric field. As a consequence, the maximum coupling strength is $g_0 = \mu_{eg}\sqrt{\omega_c/(2\hbar\varepsilon_0 V)}$. Again, the expression for the spatial distribution of the LG_{pl} mode can be given by the following relation [67,68]:

$$\mathrm{LG}_{p,l}(r, \phi) = \sqrt{\frac{2p!}{\pi(|l| + p)!}}\frac{1}{w_0}\left(\frac{\sqrt{2}r}{w_0}\right)^{|l|} L_p^{|l|}\left(\frac{2r^2}{w_0^2}\right) \times \exp\left(-\frac{r^2}{w_0^2}\right)\cos(l\phi), \tag{3}$$

where, thanks to the cylindrical symmetry of the field, we have introduced the cylindrical coordinates (r, ϕ, z), with $r = \sqrt{x^2 + y^2}$ and $\phi = \arctan(\frac{y}{x})$. $L_p^{|l|}(\frac{2r^2}{w_0^2})$ is the generalized Laguerre polynomial with radial order p and azimuthal order l. w_0 is the waist of the LG mode, which can be determined by the radius of curvature of mirrors and the cavity length.

For the sake of eliminating the explicit temporal dependence in the original Hamiltonian of Eq. (1), we would like to change the Hamiltonian into a rotating reference frame with respect to the driving field frequency ω_d by applying the unitary operator

$$\hat{U}(t) = e^{-i\omega_d t(\hat{a}^\dagger\hat{a} + \hat{\sigma}^\dagger\hat{\sigma})}. \tag{4}$$

Finally, in terms of the formula $\hat{\mathcal{H}}_{\mathrm{rot}} = \hat{U}^\dagger(t)\hat{\mathcal{H}}_{\mathrm{tot}}\hat{U}(t) - i\hat{U}^\dagger(t)\partial\hat{U}(t)/\partial t$, we can derive a time-independent effective Hamiltonian of the atom-cavity system after some algebra, with the form

$$\hat{\mathcal{H}}_{\mathrm{rot}} = \Delta_c\hat{a}^\dagger\hat{a} + \Delta_a\hat{\sigma}^\dagger\hat{\sigma} + g_e(x, y)(\hat{a}^\dagger\hat{\sigma} + \hat{a}\hat{\sigma}^\dagger) + \eta(\hat{a}^\dagger + \hat{a}), \tag{5}$$

where the notation $\Delta_c = \omega_c - \omega_d$ is the detuning of the resonance frequency ω_c of the cavity mode $\hat{a}$ from the driving field frequency ω_d (named as the cavity mode detuning). $\Delta_a = \omega_a - \omega_d$ is the detuning of the transition frequency ω_a of the two-level atom from the driving field frequency ω_d (named as the two-level atom detuning).

III. CALCULATIONS OF THE SECOND-ORDER CORRELATION FUNCTION

A. Numerical solutions via the full master equation approach

In order to describe the complete dynamics of the atom-cavity evolution in this system with the joint atom-cavity density matrix operator $\hat{\rho}$, we use the Lindblad master equation [69]

$$\frac{\partial\hat{\rho}}{\partial t} = -i[\hat{\mathcal{H}}_{\mathrm{rot}}, \hat{\rho}] + \hat{\mathcal{L}}[\hat{\rho}], \tag{6}$$

with $\hat{\mathcal{H}}_{\mathrm{rot}}$ being the effective Hamiltonian (5) under the ω_d-rotating frame of the LG-mode cavity QED system in the case of no dissipation, the notation $[\bullet, \bullet]$ being the commutation relation, and $\hat{\mathcal{L}}[\hat{\rho}]$ denoting the whole Liouvillian superoperator [70], given by

$$\hat{\mathcal{L}}[\hat{\rho}] = \frac{\kappa}{2}(2\hat{a}\hat{\rho}\hat{a}^\dagger - \hat{a}^\dagger\hat{a}\hat{\rho} - \hat{\rho}\hat{a}^\dagger\hat{a}) + \frac{\gamma}{2}(2\hat{\sigma}\hat{\rho}\hat{\sigma}^\dagger - \hat{\sigma}^\dagger\hat{\sigma}\hat{\rho} - \hat{\rho}\hat{\sigma}^\dagger\hat{\sigma}), \tag{7}$$

with the first term on the right-hand side of Eq. (7) corresponding to the damping of the cavity and the second term on the right-hand side of Eq. (7) representing the damping of the two-level atom, respectively. Here, κ is the total damping rate of the cavity (i.e., $\kappa = \kappa_L + \kappa_R$) and γ is the damping rate of the two-level atom.

By means of the connection between the Lindblad master equation and the input-output theory [69,71], we can define the operator $\hat{S}_{\mathrm{out}}$ describing the transmitted field through the right-hand cavity mirror and yield the continuity relation $\hat{S}_{\mathrm{out}} = \sqrt{\kappa_R}\hat{a}$, with κ_R the cavity damping rate through the right-hand cavity mirror. In general, for a rotating-frame time-independent Hamiltonian $\hat{\mathcal{H}}_{\mathrm{rot}}$, the dynamics of the system evolves at large times toward a steady state that satisfies the equation

$$\frac{\partial\hat{\rho}}{\partial t} = 0. \tag{8}$$

We therefore can obtain the steady-state solution $\hat{\rho}_{\mathrm{ss}}$ of the density matrix $\hat{\rho}$ for the atom-cavity system by numerically solving the equation $\partial\hat{\rho}/\partial t = -i[\hat{\mathcal{H}}_{\mathrm{rot}}, \hat{\rho}_{ss}] + \hat{\mathcal{L}}[\hat{\rho}_{\mathrm{ss}}] = 0$, with the constraint $\mathrm{Tr}(\hat{\rho}_{\mathrm{ss}}) = 1$. Here, we are particularly interested in the statistical properties of the transmitted field, which can be measured by the normalized delayed second-order intensity correlation function [72]

$$g^{(2)}(\tau) = \frac{\langle\hat{S}_{\mathrm{out}}{}^\dagger(t)\hat{S}_{\mathrm{out}}{}^\dagger(t+\tau)\hat{S}_{\mathrm{out}}(t+\tau)\hat{S}_{\mathrm{out}}(t)\rangle}{\langle\hat{S}_{\mathrm{out}}{}^\dagger(t)\hat{S}_{\mathrm{out}}(t)\rangle^2} = \frac{\langle\hat{a}^\dagger(t)\hat{a}^\dagger(t+\tau)\hat{a}(t+\tau)\hat{a}(t)\rangle}{\langle\hat{a}^\dagger(t)\hat{a}(t)\rangle^2}, \tag{9}$$

with τ the delay time between different detectors. We focus on the normalized equal-time (or zero-time-delay) second-order intensity correlation function [72], with the form

$$g^{(2)}(0) = \frac{\langle\hat{a}^\dagger\hat{a}^\dagger\hat{a}\hat{a}\rangle}{\langle\hat{a}^\dagger\hat{a}\rangle^2} = \frac{\mathrm{Tr}(\hat{\rho}_{\mathrm{ss}}\hat{a}^\dagger\hat{a}^\dagger\hat{a}\hat{a})}{[\mathrm{Tr}(\hat{\rho}_{\mathrm{ss}}\hat{a}^\dagger\hat{a})]^2}. \tag{10}$$

The second-order intensity correlation function from the output of the optical cavity can be specifically utilized to

characterize the photon bunching and antibunching [59]. More concretely, the value of $g^{(2)}(0) > 1$ [or $g^{(2)}(\tau) < g^{(2)}(0)$] represents the photon bunching corresponding to super-Poissonian photon statistics, which is a classical light and the photons are in a positive temporal correlation. On the contrary, the value of $g^{(2)}(0) < 1$ [or $g^{(2)}(\tau) > g^{(2)}(0)$] denotes the photon antibunching corresponding to sub-Poissonian photon statistics, which is a nonclassical light and the photons are in a negative temporal correlation (tending to arrive one-by-one). Also, $g^{(2)}(0) < 1$ is an important witness for the single-photon blockade effect where strong interaction between the atom and the cavity mode prevents the excitation of multiple photons at the same time [73]. In addition, the smallness of $g^{(2)}(0)$ represents the strong antibunching effect and thus can be used to characterize the quality of single-photon source [an ideal single-photon source requires $g^{(2)}(0) = 0$] [74]. In particular, the value of $g^{(2)}(0) = 1$ is referred to as the coherent-state photon corresponding to Poissonian photon statistics, which is a quasiclassical effect.

It is stressed that in general the quantum master equation cannot be solved analytically, and the numerical solutions are required. Here the second-order intensity correlation function $g^{(2)}$ in the LG-mode cavity QED system can be obtained by solving numerically Eq. (6) using a truncated Fock basis [75]. Concretely, we can truncate the largest photon number of the cavity mode in the Fock space as low as 10 for the numerical simulations in our system, which is sufficient to guarantee the precision of the numerical results for a weak drive. The details of the numerical results will be discussed in Sec. V below. Nevertheless, it should be pointed out that the analytical solutions of the second-order correlation function can help us to better explore the relationship between the correlation function $g^{(2)}(0)$ and the position of the atom. In view of this, we will discuss how to analytically calculate the second-order correlation functions $g^{(2)}(0)$ in the next section (cf. Sec. III B).

B. Analytical solutions via the Schrödinger equation approach

Now for the sake of better exploring the relationship between the second-order correlation function and the position of the atom, in this section, our main aim is to discuss how to analytically calculate the second-order correlation function $g^{(2)}(0)$ of the transmitted field. In the limit of the weak driving field, high photon excitation states have very low population and therefore we can assume the total excitation number of the atom-cavity system no more than two. Following the approach of the pure-state factorization approximation presented in Refs. [76,77], we can expand the wave function of the atom-cavity system to the two-photon excitation state with the ansatz

$$|\Psi\rangle = C_{0,g}|0,g\rangle + C_{0,e}|0,e\rangle + C_{1,g}|1,g\rangle + C_{1,e}|1,e\rangle + C_{2,g}|2,g\rangle, \tag{11}$$

where the coefficients $C_{n,g}$ and $C_{n,e}$ denote the probability amplitudes of the system in the states $|n,g\rangle$ and $|n,e\rangle$, for which the corresponding probabilities are given by $|C_{n,g}|^2$ and $|C_{n,e}|^2$, respectively. The state $|n,g\rangle$ ($|n,e\rangle$) represents n photons ($n = 0, 1, 2$) of the cavity mode at the ground state $|g\rangle$ (the excited state $|e\rangle$) of the two-level atom. Under the weak driving condition, we have the relation $C_{0,g} \gg \{C_{0,e}, C_{1,g}\} \gg \{C_{1,e}, C_{2,g}\}$.

Since we consider the weak driving limit, the atom-cavity system is rarely in the excited states and consequently the contributions of the $2\hat{a}\hat{\rho}\hat{a}^\dagger$ and $2\hat{\sigma}\hat{\rho}\hat{\sigma}^\dagger$ terms appearing in the master equation can be safely neglected. This is equivalent to acquiring the effective non-Hermitian Hamiltonian

$$\hat{\mathcal{H}}_{\rm eff} = \hat{\mathcal{H}}_{\rm rot} - i\kappa\hat{a}^\dagger\hat{a}/2 - i\gamma\hat{\sigma}^\dagger\hat{\sigma}/2. \tag{12}$$

Next, for the purpose of achieving the values of these coefficients $\{C_{n,g}, C_{n,e}\}$ to approximately calculate the second-order correlation function we are focusing on, we start from the Schrödinger equation

$$i\frac{\partial|\Psi\rangle}{\partial t} = \hat{\mathcal{H}}_{\rm eff}|\Psi\rangle. \tag{13}$$

By substituting the wave function [Eq. (11)] and the effective non-Hermitian Hamiltonian [Eq. (12)] into the Schrödinger equation [Eq. (13)], we can arrive at the evolution equations for the probability amplitudes of the wave function

$$i\frac{\partial C_{0,g}}{\partial t} = \eta C_{1,g}, \tag{14}$$

$$i\frac{\partial C_{0,e}}{\partial t} = (\Delta_a - i\gamma/2)C_{0,e} + g_e(x,y)C_{1,g} + \eta C_{1,e}, \tag{15}$$

$$i\frac{\partial C_{1,g}}{\partial t} = (\Delta_c - i\kappa/2)C_{1,g} + g_e(x,y)C_{0,e} + \eta C_{0,g} + \sqrt{2}\eta C_{2,g}, \tag{16}$$

$$i\frac{\partial C_{1,e}}{\partial t} = (\Delta_c + \Delta_a - i\kappa/2 - i\gamma/2)C_{1,e} + \eta C_{0,e} + \sqrt{2}g_e(x,y)C_{2,g}, \tag{17}$$

$$i\frac{\partial C_{2,g}}{\partial t} = 2(\Delta_c - i\kappa/2)C_{2,g} + \sqrt{2}g_e(x,y)C_{1,e} + \sqrt{2}\eta C_{1,g}. \tag{18}$$

For the case of the one-photon state, the steady-state solutions of the probability amplitudes $\{C_{0,e}, C_{1,g}\}$ can be obtained by setting $\partial C_{0,e}/\partial t = 0$ and $\partial C_{1,g}/\partial t = 0$ as

$$(\Delta_a - i\gamma/2)C_{0,e} + g_e(x,y)C_{1,g} = 0, \tag{19}$$

$$(\Delta_c - i\kappa/2)C_{1,g} + g_e(x,y)C_{0,e} + \eta C_{0,g} = 0, \tag{20}$$

where, due to the weak driving limit, the probability of finding two photons in the cavity is so small that they can be ignored relative to the probability of finding one. In this case, we can assume $C_{0,g} \to 1$, $\eta C_{1,e} = 0$, and $\eta C_{2,g} = 0$ like Ref. [78].

Using the same method, the probability amplitudes $\{C_{1,e}, C_{2,g}\}$ of the two-photon state can be expressed as

$$(\Delta_c + \Delta_a - i\kappa/2 - i\gamma/2)C_{1,e} + \sqrt{2}g_e(x,y)C_{2,g} + \eta C_{0,e} = 0, \tag{21}$$

$$2(\Delta_c - i\kappa/2)C_{2,g} + \sqrt{2}g_e(x,y)C_{1,e} + \sqrt{2}\eta C_{1,g} = 0. \tag{22}$$

Equations (19)–(22) directly illustrate the energy levels and the links between the steady states $|n,g\rangle$ and $|n,e\rangle$.

By recurrently solving Eqs. (19)–(22), we can achieve the concrete expressions for the coefficients $C_{n,g}$. Then the normalized equal-time second-order intensity correlation

function [72] based on these coefficients $C_{n,g}$ can be approximated by

$$g^{(2)}(0) = \frac{\langle\Psi|\hat{a}^\dagger\hat{a}^\dagger\hat{a}\hat{a}|\Psi\rangle_s}{(\langle\Psi|\hat{a}^\dagger\hat{a}|\Psi\rangle_s)^2} \simeq \frac{2|C_{2,g}|^2}{|C_{1,g}|^4}, \tag{23}$$

where $|\Psi\rangle_s$ is the steady-state wave function of the system. For the sake of simplicity, we define the two effective detunings $\Delta_c' = \Delta_c - i\kappa/2$ and $\Delta_a' = \Delta_a - i\gamma/2$ by including the damping rates. After straightforward calculations, we can obtain the coefficients $C_{1,g}$ and $C_{2,g}$ as follows:

$$C_{1,g} = \eta\Delta_a'\left[g_e^2(x,y) - \Delta_c'\Delta_a'\right]^{-1}, \tag{24}$$

$$C_{2,g} = \eta^2\left[(\Delta_c' + \Delta_a')\Delta_a' + g_e^2(x,y)\right]\left(\sqrt{2}\left[\Delta_c'\Delta_a' - g_e^2(x,y)\right]\left[(\Delta_c' + \Delta_a')\Delta_c' - g_e^2(x,y)\right]\right)^{-1}. \tag{25}$$

By plugging Eqs. (24) and (25) into Eq. (23), we can further derive the analytical solution of the correlation function $g^{(2)}(0)$ as

$$g^{(2)}(0) \simeq \frac{2|C_{2,g}|^2}{|C_{1,g}|^4} = \left(\left[g_e^2(x,y) - \Delta_c'\Delta_a'\right]\left[(\Delta_c' + \Delta_a')\Delta_a' + g_e^2(x,y)\right]\right)^2\left(\Delta_a'^4\left[(\Delta_c' + \Delta_a')\Delta_c' - g_e^2(x,y)\right]^2\right)^{-1}. \tag{26}$$

From the analytical expression (26) of the second-order correlation function $g^{(2)}(0)$, we can see that for the case of strong coupling [i.e., $g_e(x,y) \gg (\kappa,\gamma)$], if $(\Delta_c, \Delta_a) \sim g_e(x,y)$ and $g_e^2(x,y) \to \Delta_c\Delta_a$, then we have the result $[g_e^2(x,y) - \Delta_c'\Delta_a'] \to 0$, giving rise to $g^{(2)}(0) \ll 1$. Notice that this behavior appears only when the detunings of both the cavity mode (Δ_c) and the two-level atom (Δ_a) have the same sign [79], which provides the way for us to select the appropriate system parameters. Obviously, the second-order correlation function $g^{(2)}(0)$ is a function of the effective coupling coefficient $g_e(x,y)$, which is closely related to the specific position of the atom within the cavity. This provides a basis for the measurement of the atomic trajectory by the coherent statistics of photon antibunching.

In accordance with the previous experimental reports in Refs. [34,35], we take into account the case that the cavity damping rate κ is equal to the two-level atom damping rate γ, i.e., $\kappa = \gamma$. Again, we focus on the scenario that the detunings of the cavity mode and the two-level atom have the same sign in the strong-coupling regime, which can lead to strong antibunching. For the sake of simplicity and further illustrating the relationship between the antibunching and the atomic position, we consider that the cavity mode and the two-level atom are on-resonance, that is, $\omega_c = \omega_a$ (equivalently $\Delta_c = \Delta_a$). In these circumstances, based on Eq. (26) we can further simplify the correlation function $g^{(2)}(0)$ as

$$g^{(2)}(0) \simeq \frac{\left(\left[g_e^2(x,y) - \Delta_c^2 + \kappa^2/4\right]^2 + \kappa^2\Delta_c^2\right)\left(\left[g_e^2(x,y) + 2\Delta_c^2 - \kappa^2/2\right]^2 + 4\kappa^2\Delta_c^2\right)}{\left(\Delta_c^2 + \kappa^2/4\right)^2\left(\left[g_e^2(x,y) - 2\Delta_c^2 + \kappa^2/2\right]^2 + 4\kappa^2\Delta_c^2\right)}. \tag{27}$$

It follows from Eq. (27) that, when the effective coupling $g_e(x,y)$ and the cavity mode detuning Δ_c are equal in the strong-coupling regime, the value of the second-order correlation function is given by $g^{(2)}(0) \approx 9\kappa^2/g_e^2(x,y)$ and thus the strong antibunching can occur. The underlying physical mechanism of the strong antibunching is caused by the anharmonic energy-level spacing between different excitation states induced by the nonlinearity of the coupled atom-cavity system. Combining Eq. (2) with Eq. (3), the optimal condition $g_e(x,y) = \Delta_c$ can be further expressed as

$$\Delta_c = g_0\sqrt{\frac{p!}{(|l|+p)!}}\left(\frac{\sqrt{2}r}{w_0}\right)^{|l|} L_p^{|l|}\left(\frac{2r^2}{w_0^2}\right)\exp\left(-\frac{r^2}{w_0^2}\right)\cos(l\phi). \tag{28}$$

The above optimal condition composed of the cavity mode detuning, the maximum coupling strength, and the atomic position in the LG-mode cavity further reveals that the antibunching effect is closely related to the atomic position. The antibunching effect at the other atomic positions, where the optimal condition is not satisfied, becomes weakened. It should be pointed out that with the change of the atomic position, the physical characteristics from strong antibunching to weak antibunching enable us to detect the atomic trajectory.

The closed-form expression of the second-order correlation function $g^{(2)}(0)$ given in Eq. (27) depends on the coupling coefficient $g_e(x,y) = g_0\mathrm{LG}_{p,l}(r,\phi)/\mathrm{LG}_{0,0}(0,0)$ associated with the actual trajectory $r = \sqrt{x^2+y^2}$ [16,32,63]. When the single atom falls freely under gravity from the MOT and transits the cavity mode, the position r of the single atom is time dependent, i.e., $r(t)$, and therefore the effective coupling can be expressed as a time-dependent term that is parametrized by $g_e(t)$. In accordance with the experimental reports in Refs. [19,33–35], the off-axis distance y is an experimental constant which is determined by the falling position of the single atom (see Fig. 1) and considering that the distance between the MOT and the cavity mode is much larger than the size of the cavity mode, the velocity v of the single atom entering and leaving the cavity mode under gravity changes little and thus the velocity v of the single atom transiting the cavity mode can be assumed to be uniform (i.e., $x = vt$, and the atomic velocity can be uniquely determined based on Ref. [34]). From Eqs. (2) and (3), the time-dependent $g_e(t)$ can be written as

$$g_e(t) = g_0\sqrt{\frac{p!}{(|l|+p)!}}\left(\frac{\sqrt{2[(vt)^2+y^2]}}{w_0}\right)^{|l|} L_p^{|l|}\left(\frac{2[(vt)^2+y^2]}{w_0^2}\right)\exp\left[-\frac{(vt)^2+y^2}{w_0^2}\right]\cos\left[l\arctan\left(\frac{y}{vt}\right)\right]. \tag{29}$$

Under the θ-rotating frame coordinate transformation $x' = x\cos\theta - y\sin\theta$, $y' = x\sin\theta + y\cos\theta$ (θ is the angle between the x axis and the nodal line of the LG_{01} mode as shown in the inset of Fig. 1), the $g_e(t)$ is then given by

$$g_e(t) = g_0\sqrt{\frac{p!}{(|l|+p)!}}\left(\frac{\sqrt{2[(vt\cos\theta - y\sin\theta)^2 + (vt\sin\theta + y\cos\theta)^2]}}{w_0}\right)^{|l|}\cos\left[l\arctan\left(\frac{vt\sin\theta + y\cos\theta}{vt\cos\theta - y\sin\theta}\right)\right]$$
$$\times L_p^{|l|}\left(\frac{2[(vt\cos\theta - y\sin\theta)^2 + (vt\sin\theta + y\cos\theta)^2]}{w_0^2}\right)\exp\left[-\frac{(vt\cos\theta - y\sin\theta)^2 + (vt\sin\theta + y\cos\theta)^2}{w_0^2}\right]. \quad (30)$$

The atomic decay time is very small compared with the atomic transit time [33–35,80], which means that the system can reach the steady state in a relatively small time compared with the timescale of atomic motion. With the single atom transiting different positions of the cavity mode, the physical characteristic changing from a strong antibunching to a weak one caused by the position-dependent effective coupling makes it possible to detect the atomic trajectory by analyzing the position-dependent second-order correlation function. Therefore, we hope that the stronger the antibunching in the optimal atomic position, the greater the second-order correlation function $g^{(2)}(0)$ spectra change with the atomic position in the transit process, which makes the transit signals detected in our measurement scheme more intuitive, which will be discussed in great detail below.

IV. EXPERIMENTAL FEASIBILITY AND TYPICAL PARAMETERS FOR THE MODEL

Before proceeding, we briefly address the experimental feasibility of our scheme in Fig. 1 by means of a two-sided optical Fabry-Pérot cavity, a single alkali-metal atom, a vapor-cell MOT, and a separate external cavity diode laser (ECDL). In accordance with the experimental reports in Refs. [19,32–35,63], with approximately 10^4 atoms falling freely under gravity from the MOT initially, only one atom can transit the cavity mode of length L and Gaussian waist w_0 at a time due to the fact that the geometry of the mirror substrates can cut off most of the atomic flux, therefore the LG-mode cavity QED system can be based on the JC-type model. For example, we can employ a single ^{133}Cs atom (nuclear spin $I = 7/2$, D_2 line, and wavelength 852 nm) on the $6S$-$6P$ transition as a possible candidate [15,19] for the LG-mode cavity QED system. The designated two-level atomic states and the damping rate can be chosen as follows: $|g\rangle = |6S_{1/2}, F = 4, m_F = 4\rangle$, $|e\rangle = |6P_{3/2}, F = 5, m_F = 5\rangle$, and $\gamma = 2\pi \times 2.6$ MHz, where F denotes the hyperfine state and m_F the Zeeman substate. The atom in the states $|g\rangle = |6S_{1/2}, F = 4, m_F = 4\rangle$ and $|e\rangle = |6P_{3/2}, F = 5, m_F = 5\rangle$ can be coupled to the linearly polarized LG_{01} mode of the cavity. An external driving laser field coming from an ECDL can pump the linearly polarized cavity mode, and the frequency detuning between the external driving laser field and the $|g\rangle = |6S_{1/2}, F = 4, m_F = 4\rangle \leftrightarrow |e\rangle = |6P_{3/2}, F = 5, m_F = 5\rangle$ transition can be precisely controlled independently.

Following the method detailed in Refs. [35,81], the optical Fabry-Pérot cavity can be formed by two tapered superpolished spherical mirrors with a radius of curvature of 100 mm, an end diameter of 1 mm, and the ultrahigh reflectivity around 852 nm, which can be placed inside a no-magnet stainless-steel ultrahigh-vacuum chamber. The Fabry-Pérot cavity can be actively stabilized by using the lock laser at 828 nm, which is another longitudinal mode of the cavity via the transfer cavity technique [19]; in this way the cavity can be actively tuned into resonance with the atomic transition ($|g\rangle = |6S_{1/2}, F = 4, m_F = 4\rangle \leftrightarrow |e\rangle = |6P_{3/2}, F = 5, m_F = 5\rangle$). The locked cavity with the resonance frequency $\omega_c = 2\pi c/\lambda$ (c is the speed of light and λ is 852 nm) supports the intracavity LG_{01} mode with the waist $w_0 = 23.8$ μm. The free spectral range [82–84] of the Fabry-Pérot cavity is $\omega_{\rm FSR} = \omega_c\lambda/(2L) = \pi c/L$, where $L = 86\mu$m is the cavity length. The cavity with the linewidth (the total damping rate of the cavity mode) is $\kappa = 2\pi \times 2.6$ MHz and the finesse (roughly the number of intracavity photon round trips during the cavity decay time) is $F = \omega_{\rm FSR}/\kappa = \pi c/(\kappa L) = 6.7 \times 10^5$, thereby suggesting potentially large gains in sensitivity for sensing the atomic motion within the cavity [85].

By employing the horizon-oriented high-finesse Fabry-Pérot cavity and the ^{133}Cs MOT [19] just 5 mm above the cavity mode, we can realize the strong coupling of the individual atoms with the LG modes. The distance is much larger than the size of the cavity mode, thus the velocity of the single atom entering and leaving the cavity mode under gravity changes little and the velocity of the single atom can be assumed to be uniform during the transit time in the cavity mode. The atomic transit velocity we chose is a V-shaped distribution of the velocity of the atoms which is based on the experimental measurement [34]. The atomic transit time $w_0/v = 59.50$ μs (take $v = 0.40$ m/s as an example) is two orders of magnitude larger than the atomic decay time $2(\kappa/2 + \gamma/2)^{-1} = 0.12$ μs [80] when adopting the parameter values of $\kappa = 2\pi \times 2.6$ MHz and $\gamma = 2\pi \times 2.6$ MHz, thus the system can reach the steady state in a relatively small time compared with the timescale of atomic motion. The time-dependent effective coupling [Eqs. (29) and (30)] can be reasonably assumed to be stable on the timescale of the atomic decay like the experimental reports in Refs. [19,33–35]. Also, the position-dependent effective coupling for a standing-wave cavity mode can be reasonably set at antinode which is located at $z \approx 0$ and thus the z-axis effect can be ignored to determine the 2D position information of the atom [63]. When a system with multiple distinguishable atoms is involved, a series of meaningful works [77,80] use three-dimensional (3D) Monte Carlo simulation of an atomic beam to describe the rich physics brought by the random distribution of atomic velocity and position, the infinite hierarchy of equations alongside the effective number of atoms, and so on.

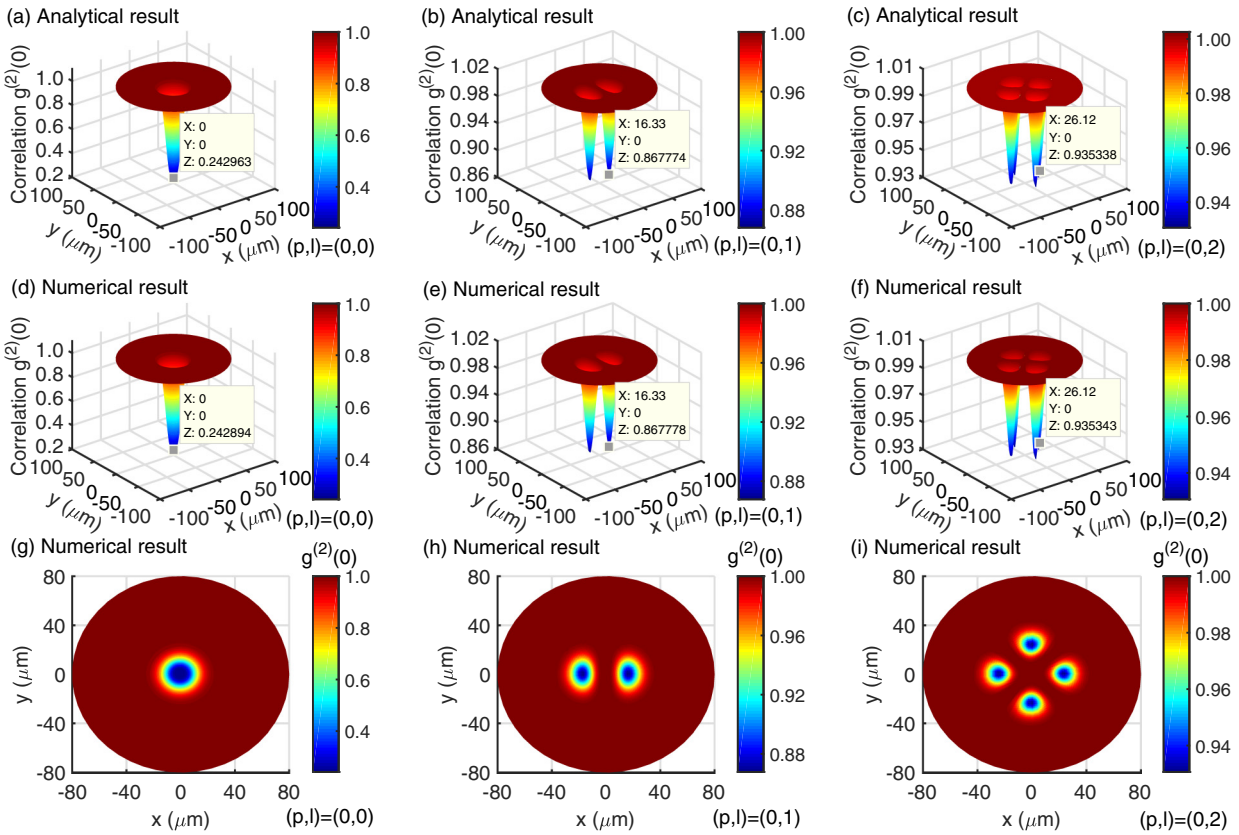

FIG. 2. The three-dimensional (3D) plots [panels (a)–(f)] and the two-dimensional (2D) plots [panels (g)–(i)] for the normalized equal-time second-order intensity correlation function $g^{(2)}(0)$ versus the positions x and y of the atom in the transverse plane when varying the LG modes (p, l) of the cavity. The top panels (a)–(c) display the 3D plots of the analytical results for the three different LG modes: (a) LG_{00} mode; (b) LG_{01} mode; and (c) LG_{02} mode. The middle panels (d)–(f) display the 3D plots of the numerical simulations corresponding to the top panels (a)–(c), respectively. The bottom panels (g)–(i) display the 2D plots of the numerical simulations corresponding to the middle panels (d)–(f), respectively. In order to avoid redundancy, the 2D plots of the analytical results are not shown here. These second-order correlation functions $g^{(2)}(0)$ are calculated numerically using the master equation (6) and also analytically using the closed-form formula (27) based on the Schrödinger equation in the steady state. The points marked in panels (a)–(f) are the values of the antibunching dips of the analytical and numerical results. The system parameters, according to the experimental data [34,35], are chosen as $g_0/2\pi = 14.3$ MHz, $\kappa/2\pi = 2.6$ MHz, $\gamma/2\pi = 2.6$ MHz, $w_0 = 23.8$ μm, $\Delta_c/2\pi = 14.56$ MHz, $\Delta_a/2\pi = 14.56$ MHz, $\eta/2\pi = 0.026$ MHz, and $\theta = 0$, respectively.

In order to better study the antibunched characteristics of the LG modes under the strong coupling, we select the typical coupling coefficient $g_0 = 2\pi \times 23.4$ MHz (and $2\pi \times 14.3$ MHz) within a reasonable range of experimental parameters [34,35,86,87]. Evidently, the coupling coefficient g_0 is larger than the cavity damping rate κ and the atom damping rate γ (i.e., $g_0 > \kappa, \gamma$), so the system can reach the strong-coupling regime of cavity QED, and under the condition of the strong-coupling regime, the atomic decay time can be very small compared to the atomic transit time. The atoms can be collected in a vapor-cell MOT directly above the center of the cavity and cooled to temperatures of $\sim$10 μK [32]. When the trapping laser beams and magnetic field in MOT are switched off, the atoms fall freely under gravity and can be transversely placed in the center plane of a single higher-order transverse LG_{01} mode. Finally, the second-order correlation function $g^{(2)}$ of the transmitted field through the right-hand cavity mirror can be measured in the same method as is done experimentally, i.e., using one ordinary 50 : 50 beam splitter and two single-photon avalanche diodes [59,73,88].

V. RESULTS AND DISCUSSIONS ABOUT POSITION-DEPENDENT PHOTON ANTIBUNCHING

First of all, we focus on the position-dependent photon antibunching features by introducing different LG modes of the cavity. To do so, the 3D plots and 2D plots for the normalized equal-time second-order intensity correlation function $g^{(2)}(0)$ in the transverse xy plane of theLG_{00}, LG_{01}, and LG_{02} modes are shown in Fig. 2. As can be seen, the LG_{00} mode exhibits only one distinct antibunching dip in the transverse plane and the minimum value of $g^{(2)}(0)$ reaches $g^{(2)}(0) \simeq 0.243$ [Figs. 2(a), 2(d), and 2(g)]. The LG_{01} mode exhibits the two antibunching dips and the minimum value of $g^{(2)}(0)$ reaches $g^{(2)}(0) \simeq 0.868$ [Figs. 2(b), 2(e), and 2(h)]. The LG_{02} mode exhibits the four antibunching dips and the minimum value of $g^{(2)}(0)$ reaches $g^{(2)}(0) \simeq 0.935$ [Figs. 2(c), 2(f), and 2(i)]. Under the same applicable system parameters, with the increase of the azimuthal order l, both the number of the antibunching dips and the minimum value of $g^{(2)}(0)$ keep increasing, which means that the antibunching effect of the system is weakened gradually. This phenomenon is mainly due to the fact that

the effective coupling between the atom and the cavity mode becomes weaker with the increase of the azimuthal order l of the LG modes, which weakens the anharmonicity of the JC ladder for the system and thus the antibunching effect. From the distribution of the antibunching dips, we can see that the distribution changes regularly with the azimuthal order l. When $l = 0$ in Figs. 2(a), 2(d), and 2(g), the antibunching dip of the system is a single dip, lying at the central position in the transverse xy plane. When $l \neq 0$ in Figs. 2(b), 2(e), and 2(h) as well as Figs. 2(c), 2(f), and 2(i), the number of symmetric antibunching dips of the system is equal to $2l$. This is because the structure of multiple lobes [89,90] associated with the azimuthal order l of the higher-order LG modes determines the effective coupling coefficient $g_e(x, y)$, and thereby affects the spatial distribution of the photon antibunching.

What is more, the numerical simulation results for the normalized equal-time second-order intensity correlation function $g^{(2)}(0)$ given by the master equation (6) are compared with the analytical results given by the closed-form formula (27) based on the Schrödinger equation in the steady state as displayed in Figs. 2(a)–(f). It is revealed from Figs. 2(a)–(f) that the values of the antibunching dips for the numerical simulations are in good agreement with those for the analytical calculations. In other words, under the condition of the weak driving field, the analytical solutions obtained by the Schrödinger equation approach in the steady state can be perfectly reproduced by the full numerical solutions achieved by the master equation approach.

In addition to these unique characteristics of the antibunching described above, Fig. 2 also reflects the dependence of photon antibunching on the atomic position. Under the different LG modes and atomic positions (x, y), the antibunching effect produced by the effective coupling is quite different. This dependence of the antibunching effect on the atomic position suggests that measuring the coherence statistics of photon antibunching can yield ample information on the atomic motion. However, there exists a limitation caused by the common symmetries of all modes [54]. For instance, a 180° rotation around the cavity axis forms a symmetry operation as shown in Fig. 2(h). Hence, using the coherence statistics of photon antibunching to track the motion of a single atom always yield two equivalent atomic paths. More than one atomic path due to the spatial symmetry of the cavity mode can emerge, which is called the trajectory degeneracy [34]. Considering that the high-order LG modes ($l > 1$) have more complex spatial symmetry structures [90], we employ the LG_{01} mode which is relatively easy to break the spatial symmetry of the atomic trajectory by the rotating frame coordinate transformation in the present work, as elaborated in detail in Sec. VI.

The antibunching effect of the LG_{01} mode can be improved by increasing the coupling strength g_0 within a reasonable experimental range [19]. As shown in Fig. 3, the simulation result referring to the LG_{01} mode reaches a value as low as $g^{(2)}(0) \simeq 0.242$ with the coupling strength increased to $g_0/2\pi = 23.4$ MHz, compared with the minimum value $g^{(2)}(0) \simeq 0.868$ when the coupling strength is $g_0/2\pi = 14.3$ MHz. In looking at the results in Fig. 3, we see that the effective coupling coefficient corresponding to the antibunching

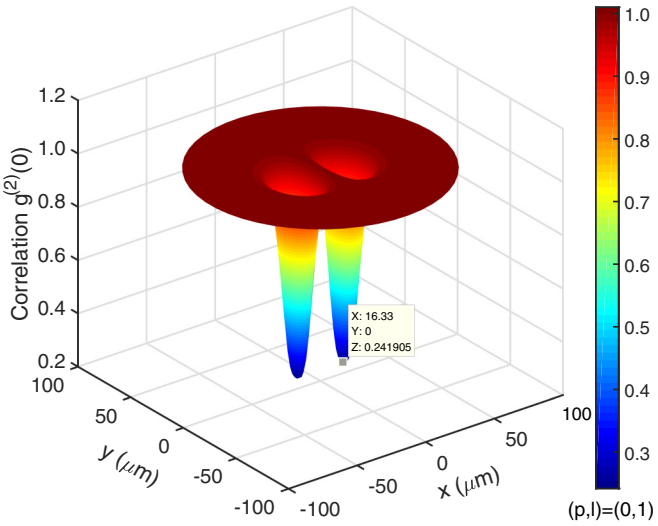

FIG. 3. The 3D plot for the normalized equal-time second-order intensity correlation function $g^{(2)}(0)$ in the transverse xy plane for the LG_{01} mode. Other system parameters are chosen as $g_0/2\pi = 23.4$ MHz, $\kappa/2\pi = 2.6$ MHz, $\gamma/2\pi = 2.6$ MHz, $w_0 = 23.8$ μm, $\Delta_c/2\pi = 14.56$ MHz, $\Delta_a/2\pi = 14.56$ MHz, $\eta/2\pi = 0.026$ MHz, and $\theta = 0$, respectively.

dip at the position $(x, y) = (16.33, 0)$ μm of the LG_{01} mode can be calculated as $g_e \times (16.33, 0)/2\pi = 14.18$ MHz. In this case, $(\Delta_c, \Delta_a) \sim g_e \times (16.33, 0)$ holds and the cavity mode detuning has the same sign as the atom detuning, thus the value of the $g^{(2)}(0)$ can be greatly reduced, as can be verified in Eq. (26). The corresponding physical mechanism is that the strong coupling between the atom and the cavity mode enhances the anharmonicity of the JC ladder for the system and thus the photon antibunching effect becomes stronger.

The degree of the photon antibunching by considering different LG modes can be characterized by the minimum value of the second-order correlation function, $g^{(2)}(0)_{\mathrm{min}}$, and the impacts of the different orders on the antibunching effect can be better understood by fixing either the radial order p or the azimuthal order l. In Fig. 4, the normalized equal-time second-order intensity correlation function $g^{(2)}(0)_{\mathrm{min}}$ versus the radial orders p (upper black abscissa axis) and the azimuthal orders l (lower red abscissa axis) are displayed. The first red-triangle dotted (upper) line corresponds to $p = 0$, $g_0/2\pi = 14.3$ MHz, and the second red-triangle dotted (lower) line corresponds to $p = 0$, $g_0/2\pi = 23.4$ MHz; they all correspond to the lower red abscissa axis and change with the azimuthal order l. From the first red-triangle dotted (upper) line, we can see that when the radial order p is fixed, $g^{(2)}(0)_{\mathrm{min}}$ keeps getting larger and tends to unity as the azimuthal order l gets higher. This is because the multiple lobes distribution of light intensity of the high-order LG modes weakens the effective coupling between the atom and the cavity mode. As can be easily seen from the comparison of the two red-triangle dotted lines in Fig. 4, the $g^{(2)}(0)_{\mathrm{min}}$ can be significantly reduced by increasing the coupling strength g_0. The first black-circle dashed (upper) line corresponds to $l = 1$, $g_0/2\pi = 14.3$ MHz, and the second black-circle dashed (lower) line corresponds to $l = 1$, $g_0/2\pi = 23.4$ MHz; they

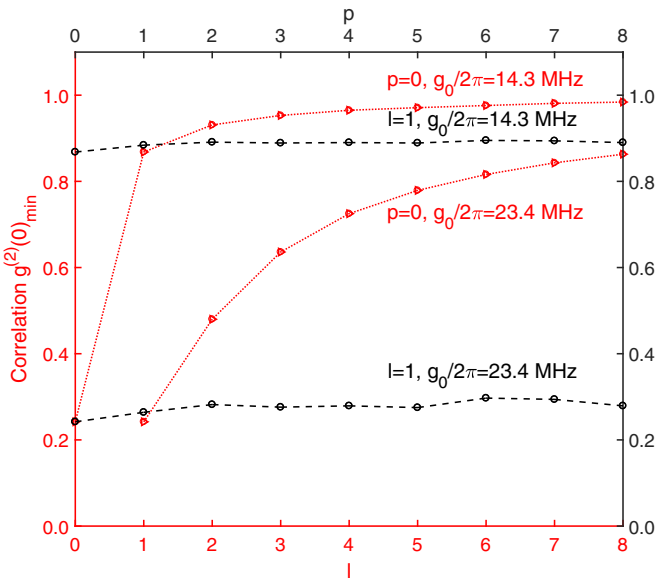

FIG. 4. The minimum of the normalized equal-time second-order intensity correlation function $g^{(2)}(0)_{\min}$ as a function of the orders p (upper black abscissa axis) and l (lower red abscissa axis). The red-triangle dotted lines correspond to the lower red abscissa axis and the black-circle dashed lines correspond to the upper black abscissa axis, respectively. The first red-triangle dotted (upper) line corresponds to $p = 0$, $g_0/2\pi = 14.3$ MHz, and the second red-triangle dotted (lower) line corresponds to $p = 0$, $g_0/2\pi = 23.4$ MHz. The first black-circle dashed (upper) line corresponds to $l = 1$, $g_0/2\pi = 14.3$ MHz, and the second black-circle dashed (lower) line corresponds to $l = 1$, $g_0/2\pi = 23.4$ MHz. Other system parameters are chosen as $\kappa/2\pi = 2.6$ MHz, $\gamma/2\pi = 2.6$ MHz, $w_0 = 23.8$ μm, $\Delta_c/2\pi = 14.56$ MHz, $\Delta_a/2\pi = 14.56$ MHz, $\eta/2\pi = 0.026$ MHz, and $\theta = 0$, respectively.

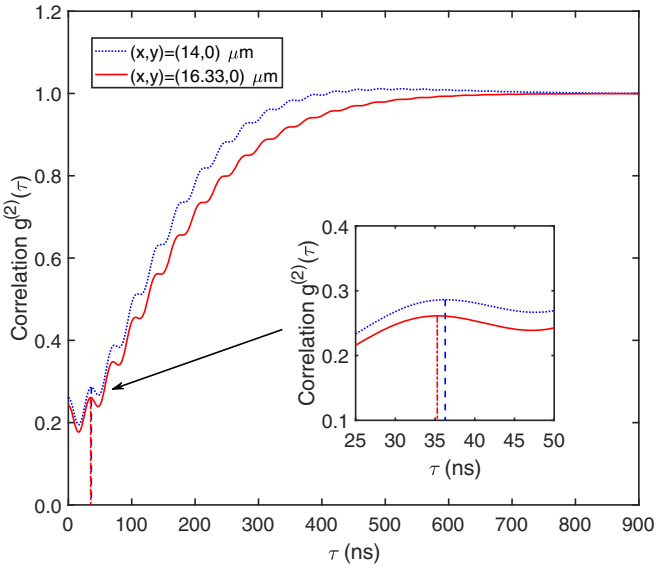

FIG. 5. The normalized delayed second-order intensity correlation function $g^{(2)}(\tau)$ at the position $(x, y) = (14, 0)$ μm (blue-dotted line) and $(x, y) = (16.33, 0)$ μm (red-solid line) of the transverse plane for the LG_{01} mode under the weak driving field. The delay time τ corresponding to the second oscillation maximum of $g^{(2)}(\tau)$ at the position $(x, y) = (14, 0)$ μm (blue-dashed vertical line) and $(x, y) = (16.33, 0)\mu$m (red-dash-dotted vertical line) are shown in the inset. Other system parameters are chosen as $g_0/2\pi = 23.4$ MHz, $\kappa/2\pi = 2.6$ MHz, $\gamma/2\pi = 2.6$ MHz, $w_0 = 23.8$ μm, $\Delta_c/2\pi = 14.56$ MHz, $\Delta_a/2\pi = 14.56$ MHz, $\eta/2\pi = 0.026$ MHz, and $\theta = 0$, respectively.

all correspond to the upper black abscissa axis and change with the radial order p. From the two black-circle dashed lines of Fig. 4, we can find that when the azimuthal order l is fixed, as the radial order p increases, $g^{(2)}(0)_{\min}$ remains unchanged. This is an advantage of using the LG modes as the transverse modes: The increase of the radial order p of the LG modes has little effect on the effective coupling coefficient, and therefore has little effect on the antibunching effect of the system. It is also revealed that the application of the LG modes can keep the system in the strong-coupling regime in a wide range of mode order. Differently from utilizing the HG modes in the previous schemes [33,35] where the effective coupling of the system and the contrast of the transit signals decrease as the mode order increases, our present method is beneficial to the mode selection of the LG modes and the maintenance of strong antibunching which can keep high contrast of the transit signals.

Although a low $g^{(2)}(0)$ ensures no simultaneous multiphoton emission, it does not reveal the time gap between the two consecutive emissions. In order to reveal the time gap between the two consecutive emissions, here we simulate the normalized delayed second-order intensity correlation function $g^{(2)}(\tau)$ at the position $(x, y) = (14, 0)$ μm (blue-dotted line) and $(x, y) = (16.33, 0)$ μm (red-solid line) of the transverse plane for the LG_{01} mode under the weak driving field, as shown in Fig. 5. The $g^{(2)}(\tau)$ characterizes the conditional probability of detecting one photon followed by another within the delay time τ. For the perfect antibunched light, the intensity correlations vanish for the short delay times. In practice, a criterion for antibunching is commonly used: the slope of $g^{(2)}(\tau)$ is positive [i.e., $g^{(2)}(\tau) > g^{(2)}(0)$], which indicates the probability for noncoincidence ($\tau \neq 0$) is bigger than coincidence ($\tau = 0$) [91]. When the delay time τ tends to zero (i.e., $\tau \to 0$), the normalized delayed second-order correlation function $g^{(2)}(\tau)$ is consistent with the normalized equal-time second-order intensity correlation function $g^{(2)}(0)$. Compared with $g^{(2)}(\tau)|_{\tau\to 0} = g^{(2)}(0) \simeq 0.261$ at $(x, y) = (14, 0)$ μm (blue-dotted line), $g^{(2)}(\tau)|_{\tau\to 0} = g^{(2)}(0) \simeq 0.242$ at $(x, y) = (16.33, 0)$ μm (red-solid line) has a small decline, that is, the antibunching effect is somewhat enhanced (cf. Figs. 3 and 5). When the delay time τ tends to infinite (i.e., $\tau \to \infty$), the normalized delayed second-order correlation function $g^{(2)}(\tau)$ can yield the limit $g^{(2)}(\tau)|_{\tau\to\infty} = 1$, which means that the system keeps the coherent state. If a system with multiple distinguishable atoms is involved, this limit can yield a value greater than unity due to the fluctuations in the effective atomic number and atomic position [77,80]. A rising slope and a strong sub-Poissonian antibunching with $g^{(2)}(0) \simeq 0.242$ indicate that the emission of a single photon occurs due to the strong blockade of multiple excitations. In Fig. 5, we can observe a rapid and small oscillation known as the vacuum Rabi oscillation that stems from the coherent energy exchange between the atom and the cavity mode [73,92]. The frequency

of the vacuum Rabi oscillation is approximately twice the effective coupling coefficient $g_e(x, y)$. The inset in Fig. 5 shows the delay time corresponding to the second oscillation maximum of $g^{(2)}(\tau)$ at the position $(x, y) = (14, 0)$ μm (blue-dashed vertical line) and $(x, y) = (16.33, 0)$ μm (red-dash-dotted vertical line). When the position changes from $(x, y) = (14, 0)$ μm to $(x, y) = (16.33, 0)$ μm, the inherent physics reflected by the tiny gap between the blue-dashed vertical line and the red-dash-dotted vertical line is accompanied by the change of the position-dependent effective coupling. From the inset we can estimate the effective coupling coefficient at $(x, y) = (14, 0)$ μm (blue-dashed vertical line) to be 13.78 MHz (corresponding to the second oscillation maximum at 36.28 ns) and the effective coupling coefficient at $(x, y) = (16.33, 0)$ μm (red-dash-dotted vertical line) to be 14.17 MHz (corresponding to the second oscillation maximum at 35.28 ns), which are in good agreement with the effective coupling coefficient obtained by the numerical calculation. The $g^{(2)}(\tau)$ in the short delay time period is small, which corresponds to a low probability of consecutive emissions.

VI. ATOMIC TRAJECTORY MEASUREMENT THROUGH POSITION-DEPENDENT PHOTON ANTIBUNCHING

As mentioned above, the normalized equal-time second-order intensity correlation function $g^{(2)}(0)$ is sensitively dependent on the position of the atom within the cavity. To this end we can use the second-order intensity correlation function of the transmitted field to determine the atomic trajectory. However, an identical spatial distribution of the antibunching dips corresponds to more than one atomic path due to the spatial symmetry of the cavity mode, which is called the trajectory degeneracy. To be more specific, for the LG_{01} mode, if the path of the cavity axis (axis z) is not considered, the left- and right-hand passing of the atom from the off-axis (axis y) can lead to the duplicate degeneracy of the atomic trajectory. In order to eliminate the trajectory degeneracy, we can take the tilted LG_{01} mode to break this symmetry by setting the angle $\theta = 15^\circ$ between the x axis and the nodal line of the LG_{01} mode (see the inset of Fig. 1; the angle can be obtained by the experiment [34]).

In this work, the trajectory of the single atom can be considered as a vertical straight line. Since the second-order correlation function $g^{(2)}(0)$ is sensitively dependent on the atomic position with the rotating coordinate transformation, we can simulate the second-order correlation function for the different trajectories of the single atom. Figure 6 shows typical correlation $g^{(2)}(0)$ spectra of the tilted LG_{01} mode. It can be easily seen from the figure that the two antibunching dips appear when the atom passes through the tilted LG_{01} mode owing to the intensity distribution of two pieces separated by a nodal line. The two antibunching dips become more asymmetric as the atomic trajectory goes further from the center of the mode [$y = \pm 5$ μm in Figs. 6(b) and 6(d) as well as $y = \pm 10$ μm in Figs. 6(a) and 6(e)], while the two antibunching dips are symmetric with $y = 0$ [see Fig. 6(c)]. When the atomic trajectory goes further from the center of the mode in the negative direction of the off-axis distance y [see Figs. 6(a) and 6(b)], the right antibunching dip is almost unchanged and the left antibunching dip gradually fades. As the left antibunching dip fades to near unity, the right antibunching dip begins to fade. Similarly, when the atomic trajectory goes further from the center of the mode in the positive direction of the off-axis distance y [see Figs. 6(d) and 6(e)], the left antibunching dip is almost unchanged and the right antibunching dip gradually fades. As the right antibunching dip fades to near unity, the left antibunching dip begins to fade. The tilted LG_{01} mode breaks the symmetric atomic trajectory degeneracy and makes it possible for us to distinguish different trajectories of the atoms. It is clear that the antibunching effect of the tilted LG_{01} mode is dependent on the parameter y, thus the trajectory of the single atom passing through the tilted LG_{01} mode can be determined uniquely.

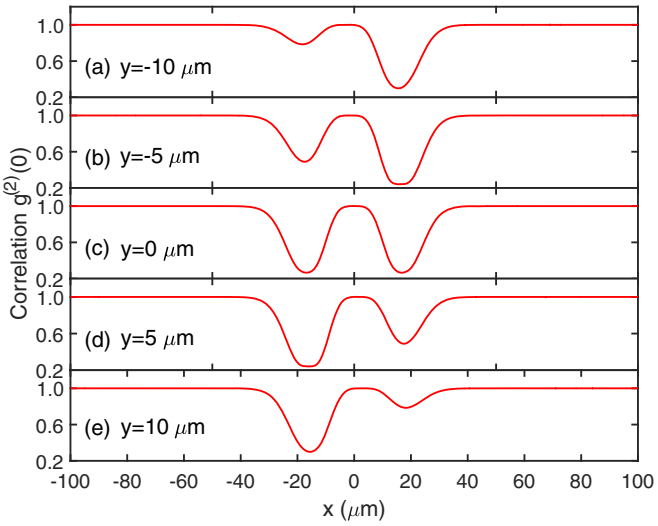

FIG. 6. The normalized equal-time second-order intensity correlation function $g^{(2)}(0)$ for the tilted LG_{01} mode as a function of the atomic position in the axis x for various off-axis distances y: (a) $y = -10$ μm; (b) $y = -5$ μm; (c) $y = 0$; (d) $y = 5$ μm; and (e) $y = 10$ μm. Other system parameters are chosen as $g_0/2\pi = 23.4$ MHz, $\kappa/2\pi = 2.6$ MHz, $\gamma/2\pi = 2.6$ MHz, $w_0 = 23.8$ μm, $\Delta_c/2\pi = 14.56$ MHz, $\Delta_a/2\pi = 14.56$ MHz, $\eta/2\pi = 0.026$ MHz, and $\theta = 15^\circ$, respectively.

Further below, we take the appropriate experimental parameters [34,35] to present the theoretical results of different atomic trajectories. The theoretical results of the normalized equal-time second-order intensity correlation function $g^{(2)}(0)$ (red-solid lines) versus the time with a single atom passing through the tilted LG_{01} mode are shown in Fig. 7. It is obvious from Fig. 7 that the two different antibunching dips can be observed, depending on the position of the atom. The two antibunching dips are symmetric when the atomic trajectory is located at $y = 0$ μm and the atomic velocity can be assumed as 0.38 m/s [see Figs. 7(b) and 7(e)]. When the atomic trajectory is not located at $y = 0$, i.e., for $y < 0$ or $y > 0$, the two antibunching dips are asymmetric, as shown in Figs. 7(a) and 7(c). For $y < 0$ in Fig. 7(a), the right antibunching dip is wider and deeper, and for $y > 0$ in Fig. 7(c), the reverse applies. Thus the atomic trajectory degeneracy can be eliminated. Figures 7(a) and 7(c) show the correlation $g^{(2)}(0)$ spectra with parameters $y = -7.3$ μm, $v = 0.40$ m/s and $y = 7.8$ μm,

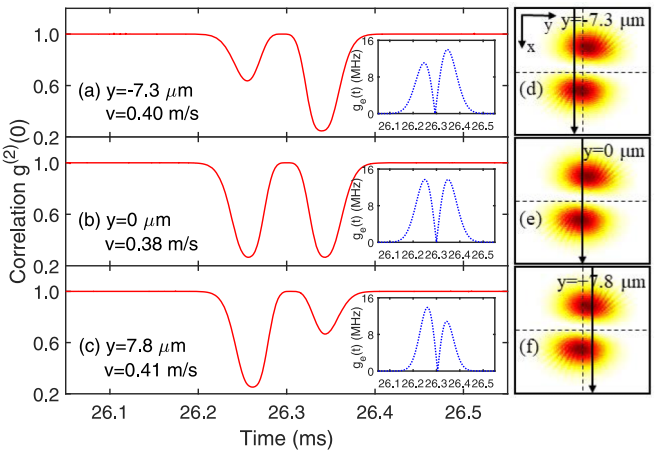

FIG. 7. The normalized equal-time second-order intensity correlation function $g^{(2)}(0)$ (red-solid lines) for the tilted LG_{01} mode as a function of the time for various off-axis distances y and atomic velocities v: (a) $y = -7.3$ μm and $v = 0.40$ m/s; (b) $y = 0$ μm and $v = 0.38$ m/s; and (c) $y = 7.8$ μm and $v = 0.41$ m/s. The right-hand panels (d), (e), and (f) show the unique atomic trajectory corresponding to the left-hand panels (a), (b), and (c), respectively. The effective coupling $g_e(t)$ (blue-dotted lines) obtained by the formula (30) as a function of the time, corresponding to the three different cases of panels (a), (b), and (c), are shown in the insets, where the insets and panels (a), (b), and (c) share the same time abscissa axis. Other system parameters are chosen as $g_0/2\pi = 23.4$ MHz, $\kappa/2\pi = 2.6$ MHz, $\gamma/2\pi = 2.6$ MHz, $w_0 = 23.8$ μm, $\Delta_c/2\pi = 14.56$ MHz, $\Delta_a/2\pi = 14.56$ MHz, $\eta/2\pi = 0.026$ MHz, and $\theta = 15^\circ$, respectively.

$v = 0.41$ m/s corresponding to a left-hand transit and a right-hand transit, respectively. The insets show the effective coupling $g_e(t)$ (blue-dotted lines) obtained by the formula (30) as a function of the time corresponding to the three different cases of Figs. 7(a), 7(b), and 7(c). The changes of the effective coupling $g_e(t)$ (blue dotted lines) correspond to the changes of the second-order correlation function $g^{(2)}(0)$ (red-solid lines). When the effective coupling is large, the antibunching is strong. So the antibunching is enhanced with the increase of the effective coupling, and vice versa. The measurement by using photon antibunching to determine the 2D position information of the atom is based on this correspondence. The break of the spatial symmetry of the tilted LG_{01} mode and the depth of the two antibunching dips allow this measurement to have good resolution for the vertical direction (axis x). Taking the theoretical simulation in a 10-μs-long time interval as an example, the spatial resolution in the vertical direction (axis x) can reach $\sim$4.0 μm. We can observe diverse correlation $g^{(2)}(0)$ spectra from Figs. 7(a) and 7(c). If $y < 0$, the atom passes through the upper part of the tilted LG_{01} mode first and then passes through the lower part [see Fig. 7(d)], and the same is true for $y > 0$ [see Fig. 7(f)]. The atomic trajectory can be uniquely determined by this tilted higher-order LG mode in the high-finesse cavity.

VII. CONCLUSIONS

In summary, we have investigated the trajectory of single atoms coupled to a tilted LG_{01} mode in a high-finesse optical cavity by using the coherence statistics of photon antibunching. Our atomic trajectory measurement scheme is based on the fact that the coherence statistics of photon antibunching carries the information about the position of the atom due to the dependence of its second-order correlation function on the position-dependent coupling strength of the atom interacting with the high-order transverse LG mode of optical cavity. Consequently, the trajectory measurement of the atom is conditioned on the detection of the antibunching transmitted photon. We compare the analytical solutions of the second-order correlation function obtained from the closed-form formulas with the numerical solutions that can be obtained from the master equation, finding that they are in good agreement. The antibunching effect of the LG_{01} mode has the unique symmetrical spatial distribution in the transverse xy plane and the robustness against the variation of radial order, which are beneficial to the mode selection of the LG modes and the single-atom trajectory measurement.

On the other hand, the trajectory degeneracy of a single atom which is hard to avoid for the usual fundamental mode can be eliminated completely due to the break of the geometry of the LG_{01} mode in the cavity. The theoretical results show that a high-finesse optical cavity can be used as a real-time single-atom detector with high spatial resolution. In a 10-μs-long time interval as an example, the spatial resolution of $\sim$4.0 μm in the vertical direction (axis x) can be achieved when an atom freely falls and is strongly coupled to the tilted LG_{01} mode. Since the cavity QED system has the capacity to give the real-time information on the measurement of the atomic position, this method seems to be an attractive technology for the experiments, e.g., the realization of an atomic kaleidoscope [54]. By combining the dynamic detection mechanism and the nature of the radiative interaction between the atom and the cavity mode [63,93], our proposed scheme may be used to develop an inversion algorithm based on the coherence statistics of photon antibunching, which can be extended to sense the kinetic energy of a single atom and the atomic center-of-mass motion in real time [32]. Better time and spatial resolution can be achieved when a smaller cavity with a larger atom-cavity coupling coefficient is utilized for measuring the 3D motion of single atoms in an optical cavity [94]. In addition to being of fundamental interest, this work may lay a foundation for the development of the time-resolved microscopy based on the strong-coupling atom-cavity microscope [63], which is broadly applicable to the monitoring of chemical and biological processes at the single-molecule scale.

ACKNOWLEDGMENTS

We are grateful to the two anonymous referees for their valuable and insightful comments in improving our paper. We also thank Xiaoxue Yang and Rong Yu for stimulating discussions. In the present research, Z.W., S.S., and J.L. were supported partially by the National Key Research and Development Program of China under Contract No. 2016YFA0301200, by the National Natural Science Foundation of China through Grant No. 11675058, and by the Fundamental Research Funds for the Central Universities,

Huazhong University of Science and Technology (HUST), under Project No. 2018KFYYXJJ037. Y.W. was supported in part by the National Natural Science Foundation of China through Grants No. 11875029 and No. 11574104.

[1] J. McKeever, A. Boca, A. D. Boozer, R. Miller, J. R. Buck, A. Kuzmich, and H. J. Kimble, Deterministic generation of single photons from one atom trapped in a cavity, Science **303**, 1992 (2004).

[2] H. J. Kimble, The quantum internet, Nature (London) **453**, 1023 (2008).

[3] A. Rauschenbeutel, G. Nogues, S. Osnaghi, P. Bertet, M. Brune, J. M. Raimond, and S. Haroche, Coherent Operation of a Tunable Quantum Phase Gate in Cavity QED, Phys. Rev. Lett. **83**, 5166 (1999).

[4] T. Wilk, S. C. Webster, A. Kuhn, and G. Rempe, Single-atom single-photon quantum interface, Science **317**, 488 (2007).

[5] B. Weber, H. P. Specht, T. Müller, J. Bochmann, M. Mücke, D. L. Moehring, and G. Rempe, Photon-Photon Entanglement with a Single Trapped Atom, Phys. Rev. Lett. **102**, 030501 (2009).

[6] D. D. Yavuz, P. B. Kulatunga, E. Urban, T. A. Johnson, N. Proite, T. Henage, T. G. Walker, and M. Saffman, Fast Ground State Manipulation of Neutral Atoms in Microscopic Optical Traps, Phys. Rev. Lett. **96**, 063001 (2006).

[7] M. G. Raizen, S. P. Wan, C. W. Zhang, and Q. Niu, Ultrahigh-fidelity qubits for quantum computing, Phys. Rev. A **80**, 030302(R) (2009).

[8] A. Kuhn, M. Hennrich, and G. Rempe, Deterministic Single-Photon Source for Distributed Quantum Networking, Phys. Rev. Lett. **89**, 067901 (2002).

[9] H. J. Kimble, Comment on "Deterministic Single-Photon Source for Distributed Quantum Networking," Phys. Rev. Lett. **90**, 249801 (2003).

[10] J. Cho, Addressing Individual Atoms in Optical Lattices with Standing-Wave Driving Fields, Phys. Rev. Lett. **99**, 020502 (2007).

[11] C. Monroe, Quantum information processing with atoms and photons, Nature (London) **416**, 238 (2002).

[12] N. Schlosser, G. Reymond, I. Protsenko, and P. Grangier, Sub-Poissonian loading of single atoms in a microscopic dipole trap, Nature (London) **411**, 1024 (2001).

[13] S. Kuhr, W. Alt, D. Schrader, M. Müller, V. Gomer, and D. Meschede, Deterministic delivery of a single atom, Science **293**, 278 (2001).

[14] M. P. A. Jones, J. Beugnon, A. Gaëtan, J. Zhang, G. Messin, A. Browaeys, and P. Grangier, Fast quantum state control of a single trapped neutral atom, Phys. Rev. A **75**, 040301(R) (2007).

[15] H. Mabuchi, Q. A. Turchette, M. S. Chapman, and H. J. Kimble, Real-time detection of individual atoms falling through a high-finesse optical cavity, Opt. Lett. **21**, 1393 (1996).

[16] P. Münstermann, T. Fischer, P. Maunz, P. W. H. Pinkse, and G. Rempe, Dynamics of Single-Atom Motion Observed in a High-Finesse Cavity, Phys. Rev. Lett. **82**, 3791 (1999).

[17] A. Haase, B. Hessmo, and J. Schmiedmayer, Detecting magnetically guided atoms with an optical cavity, Opt. Lett. **31**, 268 (2006).

[18] K. M. Fortier, S. Y. Kim, M. J. Gibbons, P. Ahmadi, and M. S. Chapman, Deterministic Loading of Individual Atoms to a High-Finesse Optical Cavity, Phys. Rev. Lett. **98**, 233601 (2007).

[19] J. M. Wang, P. F. Zhang, G. Li, and T. C. Zhang, Realization and application of strong coupling of single cesium atoms with TEM_{00} and TEM_{10} modes of a high-finesse Fabry-Perot cavity, Proc. SPIE. **8440**, 844009 (2012).

[20] P. W. H. Pinkse, T. Fischer, P. Maunz, and G. Rempe, Trapping an atom with single photons, Nature (London) **404**, 365 (2000).

[21] J. McKeever, J. R. Buck, A. D. Boozer, and H. J. Kimble, Determination of the Number of Atoms Trapped in an Optical Cavity, Phys. Rev. Lett. **93**, 143601 (2004).

[22] S. Nußmann, M. Hijlkema, B. Weber, F. Rohde, G. Rempe, and A. Kuhn, Submicron Positioning of Single Atoms in a Microcavity, Phys. Rev. Lett. **95**, 173602 (2005).

[23] H. J. Kimble, Strong interactions of single atoms and photons in cavity QED, Phys. Scr. **T76**, 127 (1998).

[24] A. Boca, R. Miller, K. M. Birnbaum, A. D. Boozer, J. McKeever, and H. J. Kimble, Observation of the Vacuum Rabi Spectrum for One Trapped Atom, Phys. Rev. Lett. **93**, 233603 (2004).

[25] J. Ye, D. W. Vernooy, and H. J. Kimble, Trapping of Single Atoms in Cavity QED, Phys. Rev. Lett. **83**, 4987 (1999).

[26] J. McKeever, J. R. Buck, A. D. Boozer, A. Kuzmich, H. C. Nägerl, D. M. S. Kurn, and H. J. Kimble, State-Insensitive Cooling and Trapping of Single Atoms in an Optical Cavity, Phys. Rev. Lett. **90**, 133602 (2003).

[27] T. Legero, T. Wilk, M. Hennrich, G. Rempe, and A. Kuhn, Quantum Beat of Two Single Photons, Phys. Rev. Lett. **93**, 070503 (2004).

[28] A. D. Boozer, A. Boca, R. Miller, T. E. Northup, and H. J. Kimble, Cooling to the Ground State of Axial Motion for One Atom Strongly Coupled to an Optical Cavity, Phys. Rev. Lett. **97**, 083602 (2006).

[29] P. Münstermann, T. Fischer, P. W. H. Pinkse, and G. Rempe, Single slow atoms from an atomic fountain observed in a high-finesse optical cavity, Opt. Commun. **159**, 63 (1999).

[30] J. A. Sauer, K. M. Fortier, M. S. Chang, C. D. Hamley, and M. S. Chapman, Cavity QED with optically transported atoms, Phys. Rev. A **69**, 051804(R) (2004).

[31] T. Pellizzari, S. A. Gardiner, J. I. Cirac, and P. Zoller, Decoherence, Continuous Observation, and Quantum Computing: A Cavity QED Model, Phys. Rev. Lett. **75**, 3788 (1995).

[32] T. W. Lynn, K. Birnbaum, and H. J. Kimble, Strategies for real-time position control of a single atom in cavity QED, J. Opt. B **7**, S215 (2005).

[33] T. Puppe, P. Maunz, T. Fischer, P. W. H. Pinkse, and G. Rempe, Single-atom trajectories in higher-order transverse modes of a high-finesse optical cavity, Phys. Scr. **T112**, 7 (2004).

[34] P. F. Zhang, Y. Q. Guo, Z. H. Li, Y. C. Zhang, Y. F. Zhang, J. J. Du, G. Li, J. M. Wang, and T. C. Zhang, Elimination of the degenerate trajectory of a single atom strongly coupled to a tilted TEM_{10} cavity mode, Phys. Rev. A **83**, 031804(R) (2011).

[35] J. J. Du, W. F. Li, R. J. Wen, G. Li, P. F. Zhang, and T. C. Zhang, Precision measurement of single atoms strongly coupled to the higher-order transverse modes of a high-finesse optical cavity, Appl. Phys. Lett. **103**, 083117 (2013).

[36] H. J. Kimble, in *Cavity Quantum Electrodynamics*, edited by P. Berman (Academic Press, San Diego, 1994).

[37] H. Mabuchi and A. C. Doherty, Cavity quantum electrodynamics: Coherence in context, Science **298**, 1372 (2002).

[38] J. M. Fink, M. Göppl, M. Baur, R. Bianchetti, P. J. Leek, A. Blais, and A. Wallraff, Climbing the Jaynes-Cummings ladder and observing its $\sqrt{n}$ nonlinearity in a cavity QED system, Nature (London) **454**, 315 (2008).

[39] B. W. Shore and P. L. Knight, The Jaynes-Cummings model, J. Mod. Opt. **40**, 1195 (1993).

[40] M. O. Scully and M. S. Zubairy, *Quantum Optics* (Cambridge University Press, Cambridge, UK, 1997).

[41] J. Kasprzak, S. Reitzenstein, E. A. Muljarov, C. Kistner, C. Schneider, M. Strauss, S. Höling, A. Forchel, and W. Langbein, Up on the Jaynes-Cummings ladder of a quantum-dot/microcavity system, Nat. Mater. **9**, 304 (2010).

[42] F. P. Laussy, E. del Valle, M. Schrapp, A. Laucht, and J. J. Finley, Climbing the Jaynes-Cummings ladder by photon counting, J. Nanophoton. **6**, 061803 (2012).

[43] H. Paul, "Photon antibunching," Rev. Mod. Phys. **54**, 1061 (1982).

[44] A. Imamoğlu, H. Schmidt, G. Woods, and M. Deutsch, Strongly Interacting Photons in a Nonlinear Cavity, Phys. Rev. Lett. **79**, 1467 (1997).

[45] B. Lounis and M. Orrit, Single-photon sources, Rep. Prog. Phys. **68**, 1129 (2005).

[46] S. Buckley, K. Rivoire, and J. Vučković, Engineered quantum dot single-photon sources, Rep. Prog. Phys. **75**, 126503 (2012).

[47] G. C. Shan, Z. Q. Yin, C. H. Shek, and W. Huang, Single photon sources with single semiconductor quantum dots, Front. Phys. **9**, 170 (2014).

[48] P. Kok, W. J. Munro, K. Nemoto, T. C. Ralph, J. P. Dowling, and G. J. Milburn, Linear optical quantum computing with photonic qubits, Rev. Mod. Phys. **79**, 135 (2007).

[49] A. Kuhn and D. Ljunggren, Cavity-based single-photon sources, Contemp. Phys. **51**, 289 (2010).

[50] E. Togan, Y. Chu, A. S. Trifonov, L. Jiang, J. Maze, L. Childress, M. V. Dutt, A. S. Sorensen, P. R. Hemmer, A. S. Zibrov, and M. D. Lukin, Quantum entanglement between an optical photon and a solid-state spin qubit, Nature (London) **466**, 730 (2010).

[51] P. Senellart, G. Solomon, and A. White, High-performance semiconductor quantum-dot single-photon sources, Nat. Nanotechnol. **12**, 1026 (2017).

[52] L. Allen, M. W. Beijersbergen, R. J. C. Spreeuw, and J. P. Woerdman, Orbital angular momentum of light and the transformation of Laguerre-Gaussian laser modes, Phys. Rev. A **45**, 8185 (1992).

[53] A. E. Siegman, *Lasers* (University Science Books, Sausalito, 1986).

[54] P. Horak, H. Ritsch, T. Fischer, P. Maunz, T. Puppe, P. W. H. Pinkse, and G. Rempe, Optical Kaleidoscope Using a Single Atom, Phys. Rev. Lett. **88**, 043601 (2002).

[55] M. Niranjan, S. Dutta, T. Ray, and S. A. Rangwala, Measuring spatially extended density profiles using atom-cavity collective strong coupling to higher-order modes, Phys. Rev. A **99**, 033617 (2019).

[56] S. Singh, Field statistics in some generalized Jaynes-Cummings models, Phys. Rev. A **25**, 3206 (1982).

[57] S. J. D. Phoenix and P. L. Knight, Establishment of an entangled atom-field state in the Jaynes-Cummings model, Phys. Rev. A **44**, 6023 (1991).

[58] J. Casanova, G. Romero, I. Lizuain, J. J. García-Ripoll, and E. Solano, Deep Strong Coupling Regime of the Jaynes-Cummings Model, Phys. Rev. Lett. **105**, 263603 (2010).

[59] K. M. Birnbaum, A. Boca, R. Miller, A. D. Boozer, T. E. Northup, and H. J. Kimble, Photon blockade in an optical cavity with one trapped atom, Nature (London) **436**, 87 (2005).

[60] Z. T. Lu, K. L. Corwin, M. J. Renn, M. H. Anderson, E. A. Cornell, and C. E. Wieman, Low-Velocity Intense Source of Atoms from a Magneto-optical Trap, Phys. Rev. Lett. **77**, 3331 (1996).

[61] K. Dieckmann, R. J. C. Spreeuw, M. Weidemüller, and J. T. M. Walraven, Two-dimensional magneto-optical trap as a source of slow atoms, Phys. Rev. A **58**, 3891 (1998).

[62] D. Plankensteiner, C. Sommer, H. Ritsch, and C. Genes, Cavity Antiresonance Spectroscopy of Dipole Coupled Subradiant Arrays, Phys. Rev. Lett. **119**, 093601 (2017).

[63] C. J. Hood, T. W. Lynn, A. C. Doherty, A. S. Parkins, and H. J. Kimble, The atom-cavity microscope: Single atoms bound in orbit by single photons, Science **287**, 1447-1453 (2000).

[64] V. I. Balykin, V. G. Minogin, and V. S. Letokhov, Electromagnetic trapping of cold atoms, Rep. Prog. Phys. **63**, 1429 (2000).

[65] M. Yu, Y. Okawachi, A. G. Griffith, N. Picqué, M. Lipson, and A. L. Gaeta, Silicon-chip-based mid-infrared dual-comb spectroscopy, Nat. Commun. **9**, 1869 (2018).

[66] C. J. Bao, P. C. Liao, A. Kordts, L. Zhang, A. Matsko, M. Karpov, M. H. P. Pfeiffer, G. D. Xie, Y. W. Cao, A. Almaiman, M. Tur, T. J. Kippenberg, and A. E. Willner, Orthogonally polarized frequency comb generation from a Kerr comb via cross-phase modulation, Opt. Lett. **44**, 1472 (2019).

[67] Y. F. Chen and Y. P. Lan, Dynamics of the Laguerre Gaussian $\mathrm{TEM}^{*}_{0,l}$ mode in a solid-state laser, Phys. Rev. A **63**, 063807 (2001).

[68] P. Fulda, K. Kokeyama, S. Chelkowski, and A. Freise, Experimental demonstration of higher-order Laguerre-Gauss mode interferometry, Phys. Rev. D **82**, 012002 (2010).

[69] C. Gardiner and P. Zoller, *Quantum Noise: A Handbook of Markovian and Non-Markovian Quantum Stochastic Methods with Applications to Quantum Optics* (Springer Science & Business Media, New York, 2004).

[70] H. P. Breuer and F. Petruccione, *The Theory of Open Quantum Systems* (Oxford University Press on Demand, New York, 2002).

[71] D. Walls and G. Milburm, *Quantum Optics* (Springer, Berlin, 1994).

[72] R. Loudon, *The Quantum Theory of Light* (Oxford University Press, Oxford, 2003).

[73] C. Hamsen, K. N. Tolazzi, T. Wilk, and G. Rempe, Two-Photon Blockade in an Atom-Driven Cavity QED System, Phys. Rev. Lett. **118**, 133604 (2017).

[74] A. Reiserer and G. Rempe, Cavity-based quantum networks with single atoms and optical photons, Rev. Mod. Phys. **87**, 1379 (2015).

[75] S. Ghosh and T. C. H. Liew, Single photons from a gain medium below threshold, Phys. Rev. B **97**, 241301(R) (2018).
[76] M. Bamba, A. Imamoğlu, I. Carusotto, and C. Ciuti, Origin of strong photon antibunching in weakly nonlinear photonic molecules, Phys. Rev. A **83**, 021802(R) (2011).
[77] H. J. Carmichael, *Statistical Methods in Quantum Optics 2: Nonclassical Fields* (Springer, Berlin, 2008).
[78] Y. L. Liu, G. Z. Wang, Y. X. Liu, and F. Nori, Mode coupling and photon antibunching in a bimodal cavity containing a dipole quantum emitter, Phys. Rev. A **93**, 013856 (2016).
[79] X. Y. Liang, Z. L. Duan, Q. Guo, C. J. Liu, S. G. Guan, and Y. Ren, Antibunching effect of photons in a two-level emitter-cavity system, Phys. Rev. A **100**, 063834 (2019).
[80] L. Horvath and H. J. Carmichael, Effect of atomic beam alignment on photon correlation measurements in cavity QED, Phys. Rev. A **76**, 043821 (2007).
[81] W. F. Li, J. J. Du, R. J. Wen, P. F. Yang, G. Li, J. J. Liang, and T. C. Zhang, Temperature measurement of cold atoms using single-atom transits and Monte Carlo simulation in a strongly coupled atom-cavity system, Appl. Phys. Lett. **104**, 113102 (2014).
[82] R. Poldy, B. C. Buchler, and J. D. Close, Single-atom detection with optical cavities, Phys. Rev. A **78**, 013640 (2008).
[83] T. F. Langerfeld, H. M. Meyer, and M. Köhl, Correlated-photon-pair emission from a cw-pumped Fabry-Perot microcavity, Phys. Rev. A **97**, 023822 (2018).
[84] D. Windey, C. G. Ballestero, P. Maurer, L. Novotny, O. R. Isart, and R. Reimann, Cavity-Based 3D Cooling of a Levitated Nanoparticle via Coherent Scattering, Phys. Rev. Lett. **122**, 123601 (2019).
[85] G. Rempe, One atom in an optical cavity: Spatial resolution beyond the standard diffraction limit, Appl. Phys. B **60**, 233 (1995).
[86] T. Fischer, P. Maunz, P. W. H. Pinkse, T. Puppe, and G. Rempe, Feedback on the Motion of a Single Atom in an Optical Cavity, Phys. Rev. Lett. **88**, 163002 (2002).
[87] A. Kubanek, M. Koch, C. Sames, A. Ourjoumtsev, T. Wilk, P. W. H. Pinkse, and G. Rempe, Feedback control of a single atom in an optical cavity, Appl. Phys. B **102**, 433 (2011).
[88] M. Mücke, J. Bochmann, C. Hahn, A. Neuzner, C. Nölleke, A. Reiserer, G. Rempe, and S. Ritter, Generation of single photons from an atom-cavity system, Phys. Rev. A **87**, 063805 (2013).
[89] A. S. Desyatnikov, D. Neshev, E. A. Ostrovskaya, Y. S. Kivshar, G. McCarthy, W. Krolikowski, and B. L. Davies, Multipole composite spatial solitons: Theory and experiment, J. Opt. Soc. Am. B **19**, 586 (2002).
[90] W. P. Zhong and L. Yi, Two-dimensional Laguerre-Gaussian soliton family in strongly nonlocal nonlinear media, Phys. Rev. A **75**, 061801(R) (2007).
[91] M. Bradford and J. T. Shen, Architecture dependence of photon antibunching in cavity quantum electrodynamics, Phys. Rev. A **92**, 023810 (2015).
[92] G. Rempe, R. J. Thompson, R. J. Brecha, W. D. Lee, and H. J. Kimble, Optical Bistability and Photon Statistics in Cavity Quantum Electrodynamics, Phys. Rev. Lett. **67**, 1727 (1991).
[93] H. Mabuchi, J. Ye, and H. J. Kimble, Full observation of single-atom dynamics in cavity QED, Appl. Phys. B **68**, 1095 (1999).
[94] Z. Q. Yin, T. C. Li, and M. Feng, Three-dimensional cooling and detection of a nanosphere with a single cavity, Phys. Rev. A **83**, 013816 (2011).